Dynamic screening effects in photoemission from oriented acetylene

Zachary H. Levine
Laboratory of Atomic and Solid State Physics, Cornell University, Ithaca, New York 14853-2501
(Received 12 February 1987)

The polarizability and photoemission cross section and asymmetry parameters for the $1\pi_u$ level of acetylene (C_2H_2) has been given previously in the time-dependent local-density approximation. In this work real-space pictures of the time-dependent potentials are given for acetylene demonstrating metalliclike screening except for energies near the previously reported autoionization resonance in the $1\pi_u$ cross section of acetylene. The character of the on-resonance screening is understood in terms of underlying molecular orbitals participating in the resonance. The differential partial cross sections for the $1\pi_u$ level are discussed in terms of the screening potentials. In general, the effect of dynamic screening is to cause the angular distribution of the outgoing photoelectrons to be enhanced in the direction of the external field.

I. INTRODUCTION

The time-dependent local-density approximation (TDLDA) has been shown to provide a good account of the photoemission cross sections[1-4] and asymmetry parameters[2-4] in atoms and molecules, as well as optical polarizabilities.[1,4-6] The approximation has also been used in a model context for jellium spheres[7,8] and semi-infinite jellium surfaces.[9] The consistent treatment of exchange and correlation between the ground and excited states as well as the existence of two sum rules shared with the true many-body system[1,10,11] on the photoemission cross section seem to be key features which account for the success of the approximation. A general feature of the photoemission spectra is that oscillator strength is shifted to higher frequencies than if the effects are omitted.[3,12] Moreover, autoionization resonances are predicted by this theory if the associated ground-state calculation is sufficiently accurate to represent the relevant one-electron levels.[1,3,10]

The local field description of screening leads to both a computational and a conceptual simplification of the dynamic screening process. The thrust of the present work is to display real-space pictures of the total potential seen by the molecule during the photoemission process for the purpose of building physical intuition about the phenomena. In addition, formalism required for the differential partial cross section is presented along with certain curves of interest near and far from the autoionization resonance in the $1\pi_u$ level. The present work is a direct extension of a previously reported study[3,4] of the cross section, asymmetry parameter, and polarizability of N_2 and C_2H_2. As such, the theory is only sketched briefly here, and the reader is referred to earlier papers[1,4,13] for details. The notation of Ref. 4 is followed strictly here.

We account for dynamic internal screening in a relatively straightforward way. The external field acting on the system is described by a scalar potential $\phi^{\rm ext}(\mathbf{r},\omega)$. In the independent-particle approximation (IPA), the induced particle density $\delta n(\mathbf{r},\omega)$ is given by the expression

$$\delta n(\mathbf{r},\omega)=\int \chi_0(\mathbf{r},\mathbf{r}',\omega)\phi^{\rm SCF}(\mathbf{r},\omega)d\mathbf{r}' ,$$

where $\chi_0(\mathbf{r},\mathbf{r}',\omega)$ is the (exact) independent-particle density-density response function in the local-density approximation to the density-functional theory (LDA). We account for internal screening of this field by recognizing that the induced charge density gives rise to an induced field equal to the sum of a Coulomb potential and an induced exchange-correlation field, i.e.,

$$\delta n(\mathbf{r},\omega)=\int \chi_0(\mathbf{r},\mathbf{r}',\omega)\phi^{\rm SCF}(\mathbf{r},\omega)d\mathbf{r}' , \quad (1)$$

where $\phi^{\rm SCF}(\mathbf{r},\omega)$ is the sum of the external field and the two induced fields just described (SCF represents self-consistent field).

The Coulomb potential is

$$\delta V_C(\mathbf{r},\omega)=e^2\int \frac{\delta n(\mathbf{r}',\omega)}{|\mathbf{r}-\mathbf{r}'|}d\mathbf{r}' , \quad (2)$$

where e is the charge on the electron. The induced exchange-correlation potential is found by linearizing the LDA exchange-correlation potential $V_{\rm xc}(\mathbf{r})$ about the ground-state value,

$$\delta V_{\rm xc}(\mathbf{r},\omega)=\frac{\partial V_{\rm xc}}{\partial n}(\mathbf{r})\delta n(\mathbf{r},\omega) . \quad (3)$$

The TDLDA consists of solving Eqs. (1)–(3) simultaneously. In the present work, these equations are solved using a molecular single-center expansion described previously.[4,13]

II. DYNAMIC SCF POTENTIALS

The nature of $\phi^{\rm SCF}(\mathbf{r},\omega)$ is illustrated in Figs. 1–4. Similar figures for atomic argon and xenon have been given previously,[1,14] as well as a related view of the effective field in acetylene.[15] Figure 1 shows the total induced potential at a low frequency for acetylene with the field oriented both parallel and perpendicular to the molecular axis. Dynamic screening reduces the polarizability from 27.30 to 5.46 Å^3 for the external field aligned with the molecular axis, and from 4.24 to 3.04 Å^3 for the perpendicular alignment,[3] compared to the experimental values[16] of 4.86 and 2.94 Å^3, respectively.

The striking feature of Fig. 1 is that there is nearly perfect or metallic screening in the region of the carbon-carbon bond for the parallel orientation of the applied field and throughout the molecular axis for the perpendicular orientation. In view of the large number of outer valence electrons available for screening, and the relatively high polarizability of the system, this behavior is not particularly surprising. Similar static screening has been reported for atomic xenon.[1] This form of the screening persists to much higher frequencies. The total potential shown in Fig. 2 for 13 eV (just below the autoionization resonance) is qualitatively similar to the low-frequency curve. The imaginary part, which represents a 90° out-of-phase component of the induced potential, is nonzero only above the photoemission threshold. It remains quite small up to this frequency.

At a calculated value of 14 eV, there is a large peak in the partial photoemission cross section arising from a coupling of the occupied $2\sigma_u$ and the unoccupied $1\pi_g$ orbitals at this photon energy.[3] The independent-particle susceptibility is given in first-order perturbation theory by

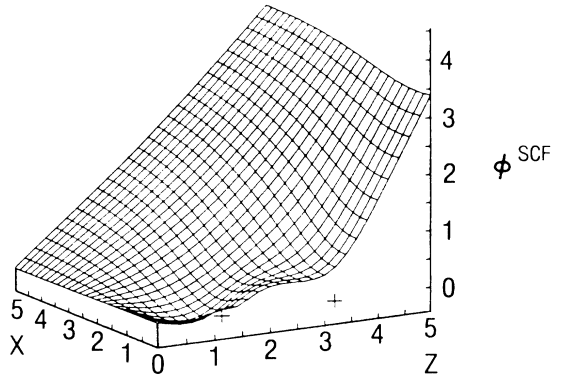

(a) $\hbar\omega = 2.7$ eV

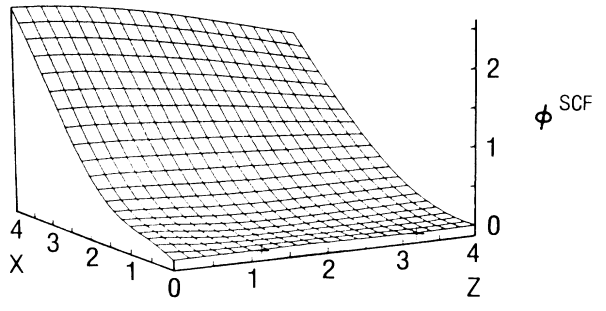

(b) $\hbar\omega = 2.7$ eV

FIG. 1. Dynamic self-consistent potential for acetylene at low frequency (2.7 eV photon energy) with external field aligned (a) parallel and (b) perpendicular to the molecular axis. The spatial unit is the Bohr radius (a_0). Below the photoemission threshold, the potential is real. Nuclear positions are denoted by plus signs; the carbon is at $z=1.13a_0$ and the hydrogen is at $z=3.19a_0$. Potential in quadrants not shown is determined by reflection symmetry.

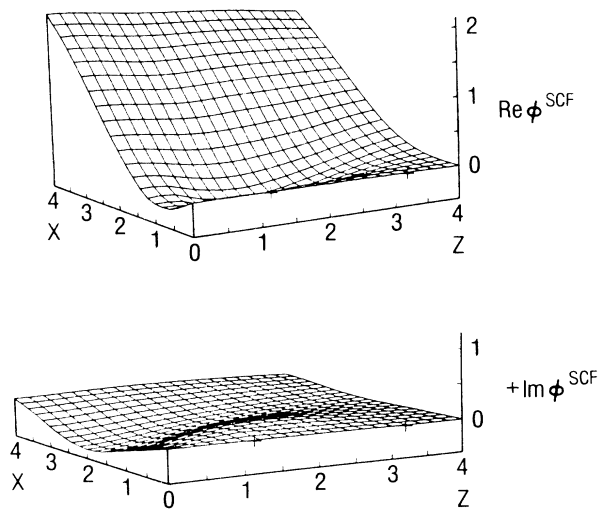

$\hbar\omega = 13$ eV

FIG. 2. Dynamic self-consistent potential for acetylene at 13 eV with external field aligned perpendicular to the molecular axis. Real and imaginary parts exist above the photoemission threshold.

$$\chi_0(\mathbf{r},\mathbf{r}',\omega)=\sum_i^{\text{occ}} \psi_i^*(\mathbf{r})\psi_i(\mathbf{r}')\sum_j \frac{\psi_j(\mathbf{r})\psi_j^*(\mathbf{r}')}{\varepsilon_i-\varepsilon_j+\hbar\omega+i\delta} + \sum_i^{\text{occ}} \psi_i(\mathbf{r})\psi_i^*(\mathbf{r}')\sum_j \frac{\psi_j^*(\mathbf{r})\psi_j(\mathbf{r}')}{\varepsilon_i-\varepsilon_j-\hbar\omega-i\delta} ,$$

where the ψ_j are single-particle orbitals with energies ε_j, and δ is an infinitesimal. Bound-state orbitals are taken to be real. When the photon energy matches the energy difference between two bound states, the denominator of the second term above vanishes except for the imaginary infinitesimal, with the numerator remaining real. The induced charge takes on a very large imaginary piece which is roughly proportional to

$$\langle 1\pi_g \mid \phi^{\text{SCF}} \mid 2\sigma_u \rangle \psi^*_{1\pi_g}(\mathbf{r})\psi_{2\sigma_u}(\mathbf{r}) ,$$

where $\phi^{\text{SCF}}(\mathbf{r},\omega)$ has the symmetry of x. The result is a large imaginary contribution to $\phi^{\text{SCF}}(\mathbf{r},\omega)$, with the real part being largely unaffected. This behavior is shown graphically in Fig. 3, where the real part is similar to the 13-eV result, but the imaginary part is resonantly large.

The situation well above the resonance is shown in Fig. 4, at 20 eV, in which the potential is given almost entirely by the external potential (which is equal to x in the real part and 0 in the imaginary part). The picture is remarkably similar to that found for $\phi^{\text{SCF}}(\mathbf{r},\omega)$ in argon and xenon above their absorption resonances[1] in that a small negative imaginary part extends over a modest region in the center of the system. Zangwill and Soven have interpreted the situation qualitatively in terms of a simple harmonic oscillator model.[14]

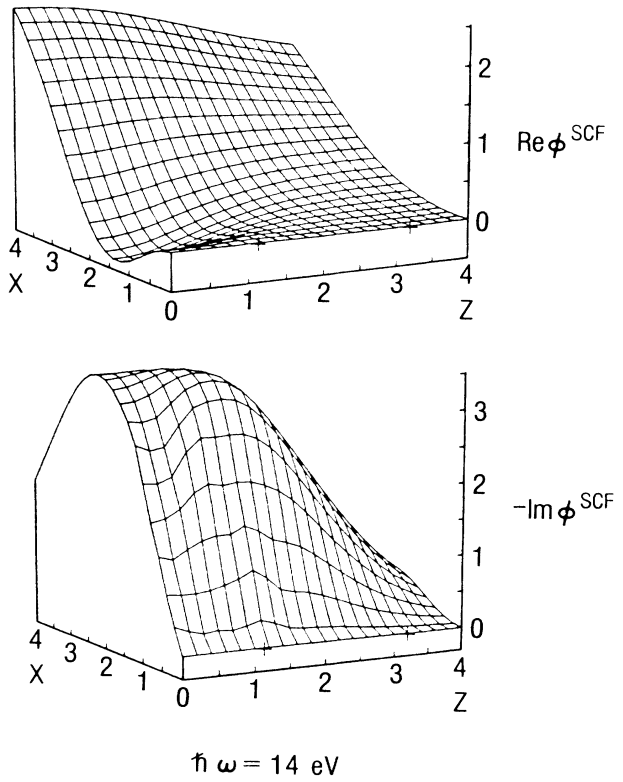

FIG. 3. Dynamic self-consistent potential for acetylene at 14 eV with external field aligned perpendicular to the molecular axis. This photon energy corresponds to the peak of the calculated total cross section.

III. DIFFERENTIAL PARTIAL CROSS SECTIONS

A. Theory

The differential partial photoemission cross section for an oriented molecule takes the form[17]

$$\frac{d\sigma_{i\hat{\mathbf{A}}}}{d\hat{\mathbf{k}}}=\frac{\alpha\hbar\omega}{4\pi}E_f^{1/2}\,|\langle\psi_i\,|\,\phi_{\hat{\mathbf{A}}}(\mathbf{r},\omega)\,|\,\psi_{\mathbf{k}}\rangle\,|^2\ ,$$

where it is assumed that the final states are plane waves plus incoming spherical waves[18] representing an electron exiting the molecule with wave vector $\mathbf{k}$. Here, i represents the one-electron level which is unoccupied in the molecular final state, $\hat{\mathbf{A}}$ characterizes the direction of polarization of the vector potential at large radius (which is parallel to the asymptotic electric field), $\hbar\omega$ is the photon energy, E_f is the final-state energy, and α is the fine-structure constant. The field may be given either in the IPA (ϕ^{ext}) or in the TDLDA (ϕ^{SCF}) and is normalized to $\phi^{\text{ext}}_{\hat{\mathbf{z}}}=z$. The formula (written in Rydberg atomic units) assumes big box normalization for the final-state wave function; asymptotically at large radius[19]

$$\psi_{\mathbf{k}}(\mathbf{r})\rightarrow e^{i\mathbf{k}\cdot\mathbf{r}}+f_{\mathbf{k}}(\hat{\mathbf{r}})\frac{e^{ikr}}{r}\ , \tag{4}$$

where the $f_{\mathbf{k}}(\hat{\mathbf{r}})$ are a set of as yet undetermined coefficients. We may write the final state as a sum over the eigenchannels $\psi_n(\mathbf{r})$,

$$\psi_{\mathbf{k}}(\mathbf{r})=\sum_n a_{\mathbf{k}n}\psi_n(\mathbf{r})\ ,$$

where n is the eigenchannel index, and $a_{\mathbf{k}n}$ are a set of constants. The eigenchannels have the following representation at large radius:[20]

$$\psi_n(r)\rightarrow\sum_L[\,\cos\delta_n\,j_l(kr)-\sin\delta_n\,n_l(kr)]Y_L(\hat{k})C_{Ln}\ , \tag{5}$$

where the δ_n are the eigenphases, L is a compact representation of the two angular momentum indices l and m, and the C_{Ln} are the eigenvectors of the K matrix.

The $a_{\mathbf{k}n}$ may be determined to be

$$a_{\mathbf{k}n}=4\pi\sum_L i^l C_{Ln}e^{i\delta_n}Y_L^*(\mathbf{k})$$

by matching the coefficients of the outgoing spherical partial waves (i.e., by matching terms of the form $(e^{-ikr}/r)Y_L(\hat{\mathbf{r}})$ in Eqs. (4) and (5). Partial-wave matrix elements I_{Lv} are given in terms of the eigenchannels as

$$I_{Lv}=\sum_n i^l C_{Ln}e^{i\delta_n}\langle\psi_i\,|\,\phi_v\,|\,\psi_n\rangle\ ,$$

where v is a polarization index on the principal axes (pointing in three orthogonal directions $\hat{\mathbf{x}}_v$) of the polarizability tensor. In terms of the partial wave matrix elements, the differential partial cross section is given as

$$\frac{d\sigma_{i\hat{\mathbf{A}}}}{d\hat{\mathbf{k}}}=4\pi\alpha\hbar\omega E_f^{1/2}\sum_{L,L',L''}C_{L'LL''}Y_L(\hat{\mathbf{k}})\times\sum_{v,v'}(\hat{\mathbf{A}}\cdot\hat{\mathbf{x}}_v)(\hat{\mathbf{A}}\cdot\hat{\mathbf{x}}_{v'})I_{L'v}I^*_{L''v'}\ , \tag{6}$$

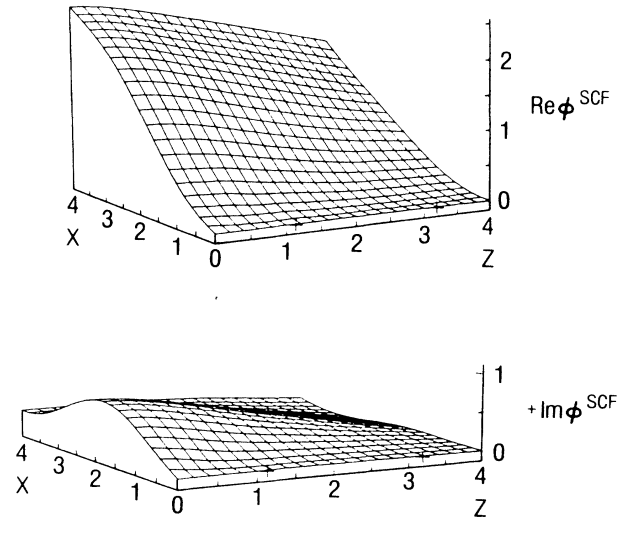

FIG. 4. Dynamic self-consistent potential for acetylene at 20 eV with external field aligned perpendicular to the molecular axis. The induced potential is small at this frequency.

where the $C_{L'LL''}=\int Y_{L'}^{*}Y_L Y_{L''}d\hat{\mathbf{k}}$ are Gaunt integrals. Note that this formula is closely related to the expression for the asymmetry parameter β given in Eq. (7) of Ref. 4. Both equations are weighted sums of the partial wave matrix elements. Naively, one would expect the quality of the predictions given in this calculation to be comparable to that of the β predictions. In Refs. 3 and 4, β was seen to be typically but not uniformly accurate to a few percent compared to experimental values.

In practice, Eq. (6) is used with keeping only a finite number of terms the sums over the eigenchannels and angular momenta. The partial cross section σ_{iv} may be found by integrating the differential partial cross section over all angles $\hat{\mathbf{k}}$. The orthonormality relations which hold among the spherical harmonics and the eigenvectors of the K matrix cause the formula to simplify to

$$\sigma_{iv}=4\pi\alpha\hbar\omega E_f^{1/2}\sum_n |\langle\psi_i|\phi_v|\psi_n\rangle|^2 .$$

Quantum interference affects the differential partial cross sections $d\sigma_{i\hat{\mathbf{A}}}/d\hat{\mathbf{k}}$ but vanish for the (integrated) partial cross sections, i.e.,

$$\sigma_{i\hat{\mathbf{A}}}=\sum_v |\hat{\mathbf{A}}\cdot\hat{\mathbf{x}}_v|^2\sigma_{iv} .$$

For cylindrically symmetric systems, we may take the molecular axis as z, and choose $\mathbf{A}$ to lie in the x-z plane, making an angle Θ_A from the z axis. In this case Eq. (6) reduces to

$$\frac{d\sigma_{i\hat{\mathbf{A}}}}{d\hat{\mathbf{k}}}=4\pi\alpha\hbar\omega E_f^{1/2}\sum_{L,L',L''}C_{L'LL''}Y_L(\hat{\mathbf{k}})[\cos^2\Theta_A I_{L'\hat{\mathbf{z}}}I_{L''\hat{\mathbf{z}}}^{*}+\sin^2\Theta_A I_{L'\hat{\mathbf{z}}}I_{L''\hat{\mathbf{x}}}^{*}+\tfrac{1}{2}\sin(2\Theta_A)(I_{L'\hat{\mathbf{z}}}I_{L''\hat{\mathbf{x}}}^{*}+I_{L'\hat{\mathbf{x}}}I_{L''\hat{\mathbf{z}}}^{*})] . \quad (7)$$

The differential partial cross section in Eq. (7) has the functional form[21]

$$\frac{d\sigma_{i\hat{\mathbf{A}}}}{d\hat{\mathbf{k}}}=\cos^2\Theta_A g_1(\theta)+\sin^2\Theta_A[g_2(\theta)+g_3(\theta)\cos(2\phi)]+\sin(2\Theta_A)g_4(\theta)\cos\phi , \quad (8)$$

where the $g_j(\theta)$ are functions which may be determined explicitly by matching terms. For σ initial states, there is a further simplification, namely, $g_2(\theta)=g_3(\theta)$, so the middle term in Eq. (8) has the form $2\sin^2\Theta_A g_2(\theta)\cos^2\phi$.

B. Results for $1\pi_u$ level of acetylene

Representative differential cross sections for the $1\pi_u$ level of acetylene are shown in Figs. 5 and 6. In Fig. 5 data are presented for the external field perpendicular to the molecular axis (i.e., $\Theta_A=90°$), hence only the term in $\sin^2\Theta_A$ is nonvanishing in Eqs. (7) and (8). The differential cross section is presented at $\phi=0°$ and $\phi=90°$, which represent the extremal values as indicated in Eq. (8). The calculation binds the $1\pi_u$ level by 7.0 eV; the final-state kinetic energy is the photon energy less this eigenvalue.

The situation at 13 eV is shown in Figs. 5(c) and 5(d). Figure 5 shows that the photoelectrons tend to exit in the equatorial plane of the molecule both in the independent-particle approximation and the TDLDA. The overall suppression of the cross section by a factor of 3 compared to the independent-particle picture is more marked for electrons exiting along the molecular axis than at the equator. If the final states are taken simply to be plane waves, it is clear that the vanishing of the external potential (by symmetry) along the molecular axis will cause the transition matrix element to be small, and the additional enhancement provided by dynamic screening will make the cross section yet smaller.

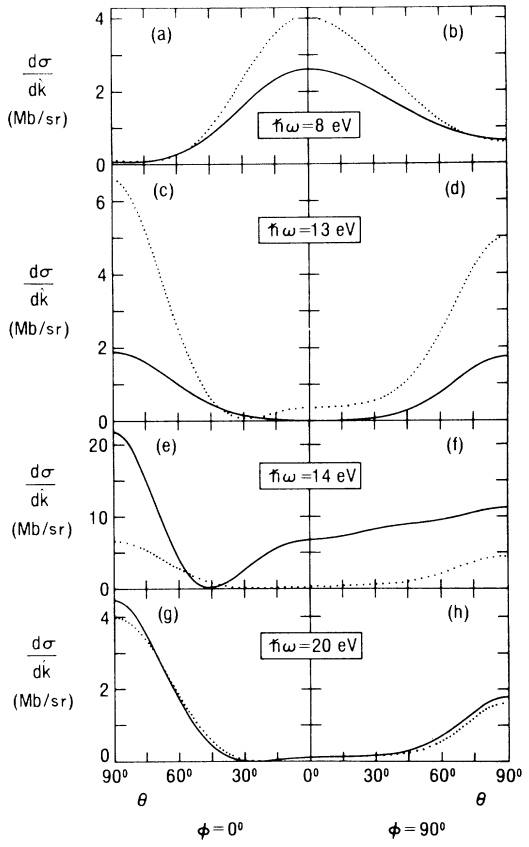

FIG. 5. Differential partial cross section for photoemission from the $1\pi_u$ level of acetylene for indicated photon energies. The external electric field is aligned perpendicular to the molecular axis ($\Theta_A=90°$). Values are given for the IPA (· · · ·) and the TDLDA (——). Panels on left (right) are for $\phi=0°$($\phi=90°$). Curves are symmetric for θ in the range of 90°–180°. Note change of scale for panels (e) and (f).

The differential cross section at the peak of the autoionization resonance is shown in Figs. 5(e) and 5(f). The independent-particle calculation is qualitatively the same as at 13 eV, but the differential cross section has a rich structure. At 20 eV [Figs. 5(g) and 5(h)], the situation returns to being principally equatorial emission. Here, the independent-particle approximation and the TDLDA are in agreement because the induced potential is negligible. Near threshold at a photon energy of 8 eV, there are strong final-state effects which cause the electrons to be ejected along the axis of the molecule, as seen in Figs. 5(a) and 5(b). The effect of dynamic screening is to reduce the magnitude of this effect somewhat, in keeping with the expected suppression of the dynamic self-consistent potential near the molecular axis.

A sample cross section for light aligned to the molecular axis is shown in Fig. 6(a) for a 13 eV photon energy. As is typical for a variety of energies, the differential cross section is peaked near 45° from the molecular axis and vanishes both on the axis and in the equatorial plane. This is a consequence of the symmetry of the initial and final states, in this case representing a π_u to π_g transition. However, as previously reported,[3,4] the principal effect of the local field is to provide cross section above threshold at all. In the independent-particle approximation, the $1\pi_u$ to $1\pi_g$ transition exhausts the oscillator strength, leaving essentially no cross section above threshold. Hence a comparison with the IPA is not really possible in this case.

Typical results for a more general angle between the external field and the molecular axis ($\Theta_A = 45°$) are seen in Figs. 6(b) and 6(c). Quantum interference effects between the parallel and perpendicular orientations are evident here. The tendency for enhanced emission parallel to the external field is seen in the enhancement of the cross section centered at $\theta = 45°$ and $\phi = 0°$. The inclusion of dynamic screening is sufficient to entirely change the character of the predicted differential cross sections in this case compared to the IPA.

IV. CONCLUSIONS

In the TDLDA, electronic correlation effects are represented by a local dynamic self-consistent potential. The use of a local potential allows for easier calculations than competitive methods, e.g., random-phase-approximation with exchange (RPAE), and also allows for intuitive understanding of the correlation process. The typical effect of the self-consistent potential at low frequencies is to screen the field in the central molecular region. However, resonant behavior may occur which may be understood in terms of particular underlying molecular orbitals.

The dynamic self-consistent potential affects the differential cross section typically by displacing the outgoing photoelectrons toward the direction of the external electric field. However, resonance or final-state effects

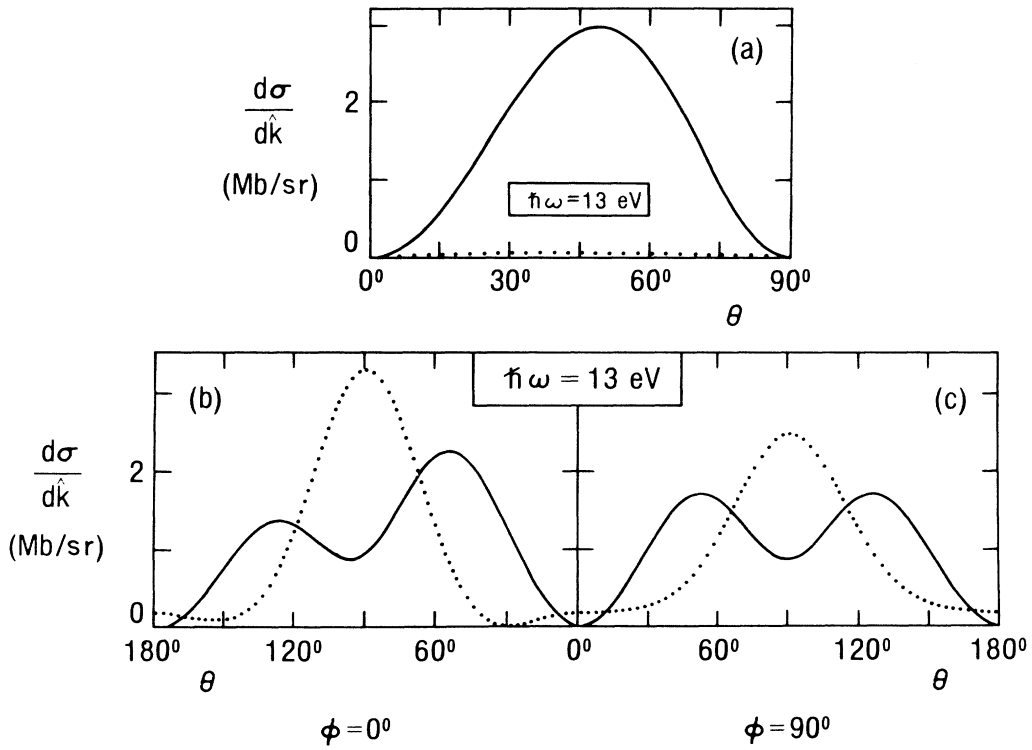

FIG. 6. Differential partial cross section for photoemission from the $1\pi_u$ level of acetylene for indicated photon energies. The external field is aligned parallel to the molecular axis in panel (a) ($\Theta_A = 0°$) and off-axis ($\Theta_A = 45°$) in panels (b) and (c). Values are given for the IPA (· · · ·) and the TDLDA (——). The curves in panels (a) and (c) are symmetric about $\theta = 90°$; the full range of θ is presented in panel (c) for ease of comparison with panel (b).

may make the picture more complicated in particular cases.

ACKNOWLEDGMENTS

I wish to thank Paul Soven and A. Zangwill for substantial assistance in conducting this research. Some of this work was performed at the University of Pennsylvania with support from the Gas Research Institute and the National Science Foundation Materials Research Laboratories Program under Grant No. DMR-79-23647 and at AT&T's Engineering Research Center with support from case 15045-15. Work at Cornell University was supported by the Department of Energy under Grant No. DEFG0Z-86ER45282.

[1]A. Zangwill and P. Soven, Phys. Rev. A **21**, 1561 (1980).

[2]F. A. Parpia, W. R. Johnson, and V. Radojević, Phys. Rev. A **29**, 3173 (1985) and references therein.

[3]Z. H. Levine and P. Soven, Phys. Rev. Lett. **50**, 2074 (1983).

[4]Z. H. Levine and P. Soven, Phys. Rev. A **29**, 625 (1984); **35**, 3964 (E) (1987).

[5]M. J. Scott and E. Zaremba, Phys. Rev. A **21**, 12 (1980); **22**, 2293 (E) (1980).

[6]G. D. Mahan, Phys. Rev. A **22**, 1780 (1980).

[7]W. Ekardt, Phys. Rev. B **32**, 1961 (1985), and references therein.

[8]M. J. Puska, R. M. Niemanen, and M. Marniner, Phys. Rev. B **31**, 3486 (1985).

[9]A. Liebsch, Phys. Rev. Lett. **54**, 67 (1985).

[10]A. Zangwill, Ph.D. thesis, University of Pennsylvania (1981).

[11]The sum rules are the f-sum rule $\int_0^\infty \sigma_\nu(\omega)d\omega=(2\pi e^2/mc)N$ and the compressibility sum rule $\int_0^\infty[\sigma_\nu(\omega)/\omega^2]d\omega=(2\pi^2/c)\alpha_\nu(0)$, where e, m, c, $\alpha_\nu(0)$, and N are the electron's charge and mass, the speed of light, the static polarizability along the ν axis, and the number of particles in the system, respectively. Hence, the accurate predictions of the static polarizability in the TDLDA have important implications for the prediction of the photoemission cross sections as well. See also U. Fano and J. W. Cooper, Rev. Mod. Phys. **40**, 441 (1980), Sec. 2.5.

[12]A. Zangwill and P. Soven, Phys. Rev. Lett. **45**, 204 (1980).

[13]Z. H. Levine, Phys. Rev. A **30**, 1120 (1984).

[14]A. Zangwill and P. Soven, J. Vac. Sci. Techn. **17**, 159 (1980).

[15]A. Zangwill and Z. H. Levine, Am. J. Phys. **53**, 1177 (1985).

[16]G. R. Alms, A. K. Burnham, and W. H. Flygare, J. Chem. Phys. **63**, 3321 (1975).

[17]This is derived from Fermi's golden rule. See, e.g., E. Merzbacher, *Quantum Mechanics*, 2nd ed. (Wiley, New York, 1970), pp. 470–481.

[18]G. Breit and H. A. Bethe, Phys. Rev. **93**, 888 (1954).

[19]The asymptotic form given here is appropriate to the neutral ground-state LDA potential. Hence, it is short ranged. The sum rules associated with TDLDA (Ref. 11) rely on the use of a single local potential throughout the calculation. The principal physical effect of omitting the Coulomb tail at large radii is to represent the high-lying bound states (e.g., Rydberg states) as part of the continuum (see Ref. 1, Sec. IV B). One obtains good agreement with experiment in TDLDA by considering photon energies rather than the kinetic energy of the final-state electron.

[20]Reference 4, Eq. (A5).

[21]J. W. Davenport, Ph.D. thesis, University of Pennsylvania (1976), p. 117. Note that whereas Davenport choses **A** to lie in the y-z plane, it is taken to lie in the x-z plane in the present work.